Molecular dynamics simulations of extended defects and their evolution in 3C-SiC by different potentials

Andrey Sarikov,[1, 2, *] Anna Marzegalli,[3] Luca Barbisan,[1] Emilio Scalise,[1] Francesco Montalenti,[3] and Leo Miglio[3]

[1] Dipartimento di Scienza dei Materiali, Università degli Studi di Milano-Bicocca, via R. Cozzi 55, 20125 Milano, Italy

[2] V. Lashkarev Institute of Semiconductor Physics, National Academy of Sciences of Ukraine, 45 Nauki avenue, 03028 Kiev, Ukraine

[3] L-NESS and Dipartimento di Scienza dei Materiali, Università degli Studi di Milano-Bicocca, via R. Cozzi 55, 20125 Milano, Italy

ORCID codes:

AS	0000-0001-9123-7203
AM	0000-0003-3109-3353
LB	0000-0002-1982-4443
FM	0000-0001-7854-8269
LM	0000-0002-1329-527X

Abstract

An important issue in the technology of cubic SiC (3C-SiC) material for electronic device applications is to understand the behavior of extended defects such as partial dislocation complexes and stacking faults. Atomistic simulations using molecular dynamics (MD) are an efficient tool to tackle this issue for large systems at comparatively low computation cost. At this, proper choice of

[*] Correspondence author. E-mail: andrey.sarikov@unimib.it

MD potential is imperative to ensure the reliability of the simulation predictions.

In this work, we compare the evolution of extended defects in 3C-SiC obtained by molecular dynamics simulations with Tersoff, analytical bond order, and Vashishta potentials. Key aspects of this evolution are considered including the dissociation of 60° perfect dislocations in pairs of 30^{O} and 90^{O} partials as well as the dependence of the partial dislocation velocity on the Burgers vector and the atomic composition of core. Tersoff potential has been found to be less appropriate in describing the dislocation behavior in 3C-SiC as compared to two other potentials, which in their turn provide qualitatively equivalent predictions. The Vashishta potential predicts much faster defect dynamics than the analytical bond order potential (ABOP). It can be applied therefore to describe the large-scale evolution of the dislocation systems and stacking faults. On the other hand, ABOP is more precise in predicting local atom arrangements and reconstructions of the dislocation core structures. In this respect, synergetic use of ABOP and Vashishta potential is suggested for the molecular dynamics simulation study of the properties and evolution of extended defects in the 3C-SiC.

Keywords: 3C-SiC, extended defects, dislocations, stacking faults, molecular dynamics simulations, LAMMPS code.

1. Introduction

Si carbide (SiC) represents a class of wide band gap semiconductor materials, which are actively studied nowadays for applications in power electronic devices with improved characteristics as compared to standard Si devices, such as faster switching speeds, lower power losses, higher blocking voltages, and higher operation temperatures. In nature, SiC is found in multiple crystalline modifications called polytypes, two of which, namely hexagonal 4H-SiC and 6H-SiC materials, are commercially available and research on the cubic polytype (3C-SiC) is an emerging field. As compared to hexagonal SiC polytypes, a number of advantages are offered by the smaller band gap (2.3 eV) and higher symmetry of the 3C-SiC phase, which include larger bulk and channel electron mobilities, increased intrinsic concentration of charge carriers, and lower density of states at the 3C-SiC/SiO_2 interface of the metal-oxide-semiconductor (MOS) device structures [1-6]. In addition, 3C-SiC layers can be easily grown on Si substrates, thus reducing significantly the layer production cost and providing high flexibility in scaling up their lateral dimensions. Low cost of 3C-SiC heteroepitaxial approach and high scalability to 300 mm and even larger Si wafers makes this technology extremely competitive for the hybrid electric vehicles, air conditioning, and LED lighting system applications.

At the same time, many open issues still remain for the development of high-performance devices based on 3C-SiC epi-layers related to the presence of extended defects in this material. For 3C-SiC grown on Si substrates, such defects as micro-twins, antiphase boundaries, misfit dislocations and stacking faults extend from the 3C-SiC/Si interface resulted from the lattice constant and thermal expansion coefficient mismatch between the two materials [7]. Although most of these defects reduce their density or even disappear in very thick (several tens of microns) 3C-SiC epitaxial films, the net defect density never falls to zero [7, 8]. In addition, extended defects may generate during the 3C-SiC film growth induced by local strain fields as well as mistakes in the crystal layer ordering [8, 9].

3C-SiC has zinc-blend crystal structure, in which partial stress release is achieved by a

formation of 60^O perfect dislocations in the glide set of crystal lattice. For example, for the direction of the dislocation line $\mathbf{l} = \left|110\right|$, its Burgers vector corresponds to $\mathbf{b}_{60} = \frac{1}{2}\left[011\right]$. Following the energy minimization pathway, 60^O perfect dislocations can further dissociate into pairs of 30^O and 90^O Shockley partials (the Burgers vectors $\mathbf{b}_{30} = \frac{1}{6}\left[121\right]$ and $\mathbf{b}_{90} = \frac{1}{6}\left[\bar{1}12\right]$, respectively, for the exemplary 60^O dislocation mentioned above), bordering the stacking faults (SFs) formed between them [10-12]. These stacking faults are characterized by high electrical activity due to segregation of doping impurities and belong therefore to the most important extended defects in 3C-SiC material [13-15]. For example, the experimental results by Nagasawa et al. demonstrate that an increase of the linear density of stacking faults by an order of magnitude leads to an increase in the leakage current density of 3C-SiC based devices about three orders of magnitude at 600 V [16, 17]. Stacking faults reveal complex behavior during 3C-SiC layer growth and processing, which includes SF generation as well as stopping without interaction with other SFs, as demonstrated by transition electron microscopy (TEM) investigations [7]. Understanding this behavior is imperative for improvement of a control and manipulation of SF distribution and, hence, the electric characteristics of 3C-SiC devices. In addition, more complex defects in 3C-SiC such as twin regions, polytype inclusions and antiphase domains include the stacking faults and bounding partial dislocations as their building blocks. Therefore, studies of the latter may give an insight in the mentioned complex defects properties and behavior.

Because of the long-range stress fields, created by the dislocations and determining the evolution in the dislocation containing systems, modeling of the latter with sufficient reliability of predictions requires atomistic simulations at the time scales and for the system sizes, which cannot be treated by *ab initio* simulation methods. Molecular dynamics (MD) simulations can be an appropriate solution to study the evolution of the stacking faults and dislocations in 3C-SiC epitaxial layers. MD simulation method has a number of advantages over other approaches. On the one hand, it enables to track the evolution of the systems under investigation at atomic scale. On the

other hand, use of effective potentials describing the atomic or molecular interaction, in the framework of the Newton mechanics makes MD calculations much faster than the more fundamental *ab initio* calculation approaches thus enabling to operate much higher numbers of atoms and larger system sizes. As compared to lattice kinetic Monte Carlo approaches, which may be used to model the same tasks, molecular dynamics does not require time consuming model calibrations.

It should be always remembered, however, that the potentials used for molecular dynamics simulations being empirical should not be regarded as universally applied or quantitatively precise so that the best potential choice for particular task is often required. A number of potentials have been proposed for MD simulations of SiC materials [18-22], which have been successfully applied to study the fundamental SiC characteristics as well as the SiC structural phase transformations under pressure [23], behavior of SiC ceramics under shock loading [24, 25], and nanoscale plasticity of single crystal 3C–SiC during nanometric cutting [26, 27].

A number of publications has been devoted to the MD simulation studies of the formation and evolution of extended defects in 3C-SiC induced by external mechanical impact [24-27]. In these studies, defect networks with high amounts of dislocations and stacking faults are considered macroscopically, ignoring the details of individual dislocation interaction as well as evolution of local atomic configurations of the dislocation cores. For the mentioned kind of problems, the potential proposed by Vashishta et al. [22], reproducing the most accurately the generalized stacking fault energy (GSFE) and mechanical characteristics of 3C-SiC, has demonstrated its superior efficiency over other MD potentials.

At the same time, however, in 3C-SiC layers epitaxially grown on Si substrates understanding the interaction of individual partial dislocations and formation of local atomic configurations of dislocation complexes becomes more important. Therefore, an independent test of the applicability of classical potentials to meet the requirements to tackle these issues by molecular dynamics simulations, is desirous. To the best knowledge of us, a comparison between Vashishta

and other MD potentials in describing individual defects and processes at atomic scale was never reported.

In this work, we perform comparative molecular dynamics simulation study of the evolution of the systems consisting of 60^{O} perfect and 30^{O} and 90^{O} Shockley partial dislocations as well as stacking faults in 3C-SiC material with three potentials, namely Tersoff [20], analytical bond order [21] and Vashishta potential [22]. We make a detailed analysis of the capabilities offered by each potential as well as their restrictions in application to describe the structures and dynamics of extended defects in 3C-SiC. Based on this study we suggest an MD simulation approach in terms of the potentials used, to model various types of extended defects, including dislocations and stacking faults as well as their complexes, in cubic silicon carbide layers.

2. Methodology

Comparative study of the dynamics of dislocations and stacking faults in cubic SiC phase (3C-SiC) has been performed using molecular dynamics (MD) simulations with different potentials describing the interaction of Si and C atoms. In particular, behaviors of mentioned defects obtained with Tersoff [20], analytical bond order potential (ABOP) introduced by Erhart and Albe [21], and Vashishta potential [22] have been compared. We do not present here mathematical expressions describing these potentials as the adequate mathematical presentation would require reproducing the main contents of the original publications [20-22] and overload the text of this paper. Interested readers are directed therefore to the publications [20-22] to get full insight into the mathematical details of the potentials.

Tersoff potential and ABOP are the bond order potentials [28] formulated in terms of repulsive and attraction interactions between the atoms, whose extension is limited to the first coordination sphere by respective choice of the cut-off functions. For this reason they are inapplicable to characterize the energy difference between SiC polytypes, which have identical first-neighbor atom arrangements. In its turn, Vashishta potential for silicon carbide is based on the

modification of the Stillinger-Weber form proposed for Si [29] to describe structural transformations under pressure and melting behavior of SiC materials maintaining at the same time the bond-bending and bond-stretching characteristics. Due to its cut-off distance r_c = 7.35 Å, far beyond the cut-off ranges of both Tersoff potential and ABOP, the geometrical arrangement of second nearest neighbors in the crystal lattice is taken into account in energy calculations with Vashishta potential, so that different SiC polytypes are distinguished from the potential energy point of view.

The functional form of the Tersoff potential and ABOP for silicon carbide comprise the coefficients of the interaction of Si–Si and C–C atoms in addition to the Si–C interaction. This means that apart from the SiC itself, the same potentials may be used to model elementary silicon and carbon materials. Unlike them, no such possibility is offered by the Vashishta potential due to the repulsion between the same-type atoms conditioned by the parameter values of its two-body term and zero value of the three-body term for Si–Si–* or C–C–* sequences (asterisk substitutes any of the C and Si atoms).

MD simulations have been performed using the Large-scale Atomic/Molecular Massively Parallel Simulator (LAMMPS) code [30] in the canonical ensemble (N, V, T), using a Nose-Hoover thermostat regime at the temperatures ranging from 1200 to 2000 K. These simulation temperatures have been chosen as satisfying the following conditions: (i) to be not too much different from the actual temperatures of 3C-SiC layer deposition (~ 1300 – 1600^{O}C), (ii) to be sufficiently high for the defect evolution could be observed without need to perform unreasonably long simulations, which is achieved in the upper limit of the used temperature range, and (iii) to be well below the 3C-SiC melting temperature predicted by each of the potentials (~ 3250 K for Vashishta potential [22] and ~ 3800 K for Tersoff potential and ABOP [31], respectively) to avoid possible influence of the pre-melting lattice disorder on the defect dynamics.

The value of the time step has been chosen equal to 0.3 fs based on the energy conservation of simulation system in the course of microcanonical simulation runs. To avoid the temperature

shock effect on the 3C-SiC system, the value of temperature was increased from 300 K up to the targeted high temperature value during 1.5 ps of simulated time. MD simulations have been carried out applying the periodic boundary conditions on all sides of the box-shaped simulation cell bounded by the planes with orientations $[1\bar{1}\bar{2}]$, $[1\bar{1}1]$, and $[110]$ in the directions of the axes *X*, *Y*, and *Z*, respectively. Prior to the temperature increase in the course of simulations, the system has been allowed to relax using the LAMMPS energy minimization procedure with the Polak-Ribiere conjugate gradient algorithm (stopping tolerance for energy and force were equal to 10^{-6} and 10^{-8} eV/Å, respectively). Analysis of the dislocation structures in the 3C-SiC systems obtained at various time steps has been performed using the Open Visualization Tool (OVITO) software [32].

The dislocations have been inserted into the simulation cells with initially perfect crystalline structure by displacing all the cell atoms by the vectors the components of which have been calculated in the framework of the dislocation theory [33] as follows:

$$u_x = \frac{b_{edge}}{2\pi}\left[\tan^{-1}\frac{y}{x} + \frac{xy}{2(1-\nu)(x^2+y^2)}\right] \tag{1.1}$$

$$u_y = -\frac{b_{edge}}{2\pi}\left[\frac{1-2\nu}{4(1-\nu)}\ln(x^2+y^2) + \frac{x^2-y^2}{4(1-\nu)(x^2+y^2)}\right] \tag{1.2}$$

$$u_z = \frac{b_{screw}}{2\pi}\tan^{-1}\frac{y}{x} \tag{1.3}$$

where b_{edge} and b_{screw} are the edge and screw components of the dislocation Burgers vector, respectively, $\nu = 0.25$ is the 3C-SiC Poisson ratio [34], and *x*, *y*, and *z* are the atom coordinates, respectively. The correspondence between the directions of the *X*, *Y* and *Z* coordinate axes as well as the orientations of the components of dislocation Burgers vector are shown in Fig. 1.

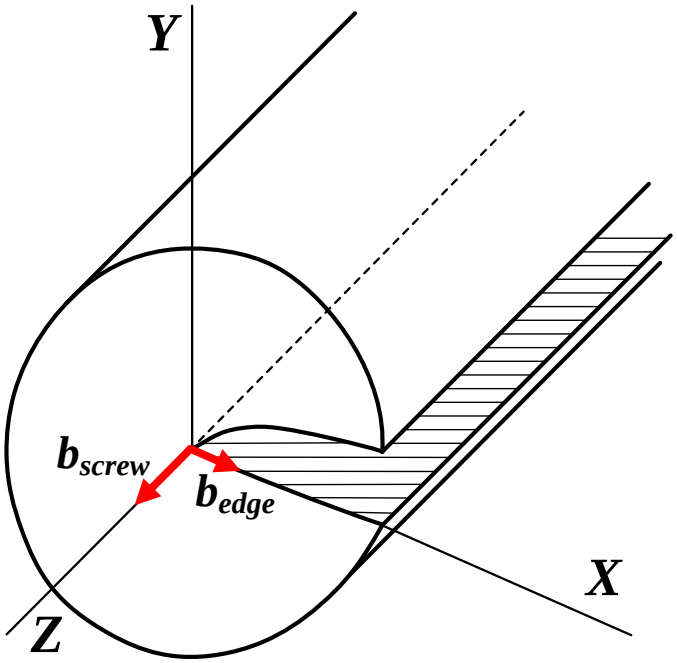

Fig. 1 Schematic representation of the dislocation in the 3C-SiC phase containing screw and edge components

Insertion of a single dislocation would lead to the appearance of an atomic step on the simulation cell boundary plane induced by atom shifting. Therefore, to preserve the integrity of simulation cell boundaries, perfect or partial dislocations with opposite Burgers vectors were always inserted in pairs into the same $[1\bar{1}1]$ plane perpendicular to the *Y* axis with some in-plane separation between them. Such dislocations with opposite Burgers vectors considered together are referred to as dislocation dipole. Various separation distances and simulation cell sizes have been probed to find the optimum values of these quantities with respect to the reliability of modeling predictions on the one hand, and simulation speed on the other hand. In particular, for each trial simulation run the cell dimensions from the preceding run have been doubled in alternation with doubling the distance between the inserted dislocations. The simulation cell size and the distance between the dislocations have been chosen so that doubling these quantities made no effect on the dislocation behavior during probe MD simulations. Based on this study, a cell with 24576 atoms in total sized as $24\times\frac{\sqrt{6}}{6}4a \times 4\times\frac{\sqrt{3}}{3}6a \times 4\times\frac{\sqrt{2}}{2}2a$, and the distance between the dislocations equal

to $18\times\frac{\sqrt{6}}{2}a$, where a is the potential dependent lattice constant of 3C-SiC material, have been chosen for the demonstration of simulation results.

3. Results

3.1. Properties of 3C-SiC with MD potentials

Prior to the study of the evolution of extended defects in 3C-SiC by molecular dynamics simulations with potentials described above, the latter have been comparatively tested with respect to their predictions of some of the basic 3C-SiC characteristics. In particular, for each potential we have determined the lattice parameter a and cohesive energy E_C as the values corresponding to the minimums in the dependences $E_C(a)$ calculated applying the LAMMPS energy minimization procedure at each value of a. Table 1 shows the values of the lattice constant and cohesive energy of 3C-SiC calculated using three MD potentials and compared to respective experimentally determined values. It can be seen that all three potentials demonstrate satisfactory predictive power for these quantities. There are almost no discrepancies between the experimental and calculated results for ABOP and Vashishta potential, while Tersoff potential shows small underestimation of the value of 3C-SiC lattice constant by about 1.9 % and overestimation of the cohesive energy value by approximately 1.4 %, respectively. To better demonstrate the predictive power of all three potentials, we have also determined the values of the lattice constants of hexagonal 2H-SiC phase, which are calculated over the equivalent cubic lattice constant a as follows:

$$a^* = \frac{a}{\sqrt{2}}, \qquad c^* = \frac{2a}{\sqrt{3}} \tag{2}$$

as well as its cohesive energy. The results presented in Table 1 demonstrate the equal values of the determined quantities for 3C and 2H SiC phases in case of Tersoff potential and ABOP, which is a consequence of the limitation of the latter by the interactions within the first coordination sphere.

On the other hand, the equivalent lattice constant and cohesive energy determined with Vashishta potential are smaller for 2H-SiC as compared to those of 3C-SiC phase, resulted from the account of longer-range atom interaction by this potential. As in the case of 3C-SiC, ABOP and Vashishta potentials demonstrate much better agreement of calculated values with respective experimental data.

Table 1. Calculated and experimental values of selected physical quantities of 3C-SiC phase

	Tersoff potential	ABOP	Vashishta potential	Experiment
3C-SiC				
Lattice constant (Å)	4.2796	4.3593	4.3582	4.3596 [35]
Cohesive energy (eV/atom)	6.4338	6.3392	6.3401	6.34 [36]
2H-SiC				
Lattice constants (Å)				
a^*	3.0261	3.0825	3.0647	3.0763 [37]
c^*	4.9417	5.0337	5.0046	5.0480 [37]
Equivalent cubic lattice constant	4.2796	4.3593	4.3341	
Cohesive energy (eV/atom)	6.4338	6.3392	6.3209	

In addition to the above mentioned 3C-SiC characteristics, the specific energy of a single (or intrinsic) stacking fault has been calculated with each of the considered MD potentials. In the cubic crystal lattice, intrinsic stacking fault is formed by a removal of a double plane from the ABC plane sequence along the [111] direction, thus creating an inclusion with hexagonal wurzite configuration in the zinc-blend structure of the 3C-SiC phase. Intrinsic stacking faults are closely related to the partial dislocations as the boundaries between the former and the surrounding perfect crystal in the

stacking fault plane [12].

The values of the stacking fault energy in 3C-SiC have been calculated subtracting the potential energy of the stacking faulted configuration from that of the corresponding perfect cubic lattice. The energy cost per unit area of a single stacking fault calculated with Vashishta potential is equal to 12.09 meV/Å^2. This value is overestimated as compared to the respective energy of 2.51 meV/Å^2 provided by the latest DFT calculations [38], and 2.12 meV/Å^2 obtained from experimental results [39, 40]. Despite this discrepancy, no better estimation can be obtained with existing semi-empirical MD potentials. It should be also noticed that values of the stacking fault energy determined both by DFT and using Vashishta potential are of the same sign and will influence the energy of 3C-SiC system with the extension or shrinking of the stacking fault in the same way. In particular, positive energy contribution will affect the evolution of the systems containing stacking faults during MD simulations with Vashishta potential tending to decrease the stacking fault extension. In their turn, both Tersoff potential and ABOP, being limited to the first coordination sphere, make no difference between the hexagonal wurzite and cubic zinc-blend SiC configurations therefore predicting zero value of the stacking fault energy.

3.2. Stability of dislocation core reconstructions with MD potentials

In [12, 41], peculiar reconstructions of the cores of 30^O and 90^O partial dislocations in 3C-SiC have been reported, obtained by density functional theory (DFT) calculations. In this work, we analyze the capability of three used MD potentials to maintain the atomic configurations of the reconstructed dislocation cores. To do this, the coordinates of the atoms corresponding to the 2×1 core reconstruction of the 30^O partial dislocations as well as to the single period reconstruction of the 90^O partial cores have been obtained first using the DFT approach at the generalized-gradient approximation (GGA) level [38]. The resulting core configurations fully agree with those obtained in [12, 41] and are shown in Fig. 2 a and e for the 30^O and 90^O partial dislocations, respectively.

The DFT reconstructed dislocations have been replicated into the simulation cell followed

by energy minimization with MD potentials. As can be seen from Fig. 2 b – d, f – h, the core reconstructions are maintained by only Tersoff potential and ABOP, while noticeable transformations of the cores of partial dislocations occur as a result of energy minimization with Vashishta potential (see Fig. 2 d and h). In particular, 30^{O} partial dislocations lose the 2×1 core reconstruction and the internal core atoms become located in the equidistant positions. In the case of 90^{O} partials, slight shift of the stacking faulted plane (right from the dislocation core) parallel to the dislocation line takes place so that the distances between the neighboring Si atoms in the dislocation core become equal, and so do the distances between the neighboring C atoms. The reason for such behaviors provided by the Vashishta potential is the repulsion between the atoms of the same types imposed by its mathematical structure, which drives them to separate each from other at the largest achievable distance.

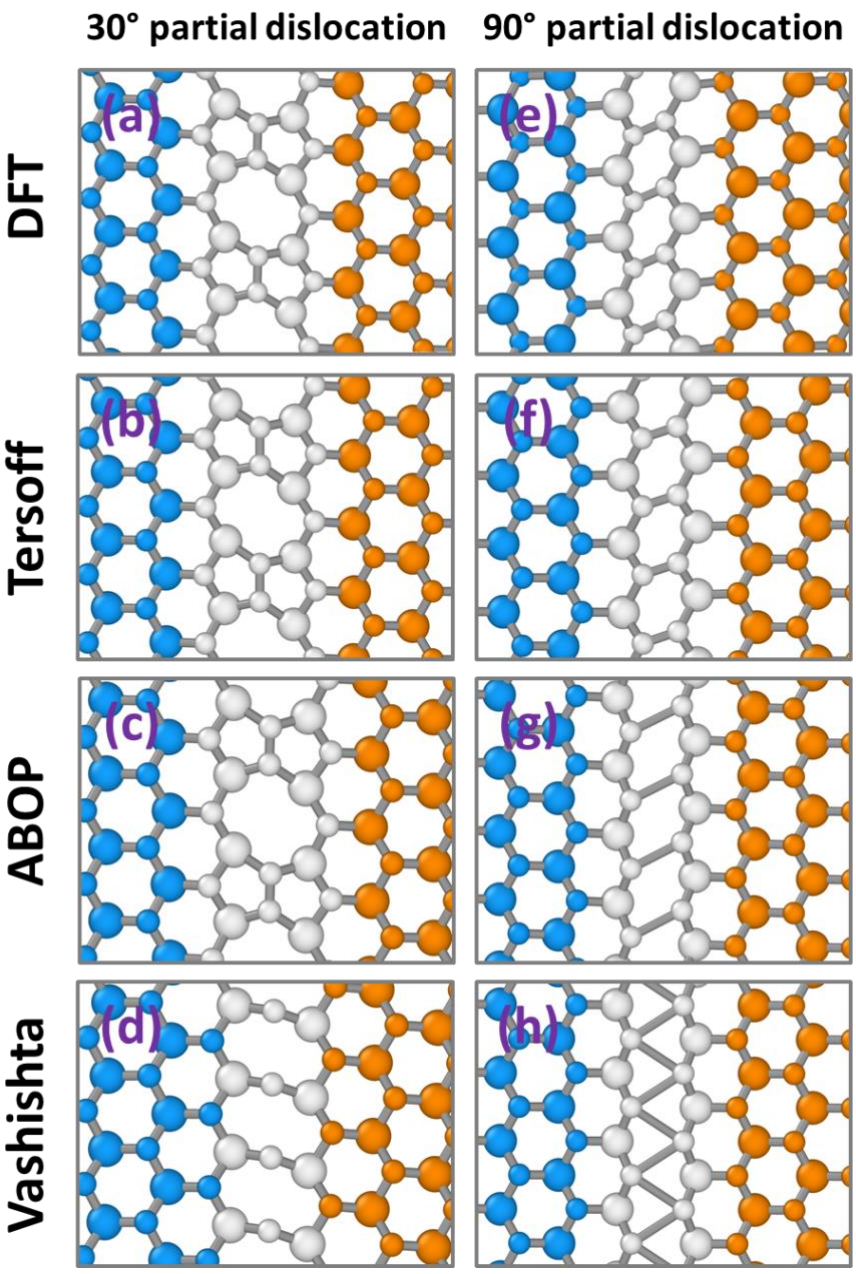

Fig. 2 Top view of the atomic configurations of the cores of 30^O (a – d) and 90^O (e – h) Shockley partial dislocations obtained by DFT calculations (a, e) as well as after energy minimization procedure with Tersoff potential (b, f), ABOP (c, g), and Vashishta potential (d, h), respectively. Larger spheres represent Si atoms, while smaller ones correspond to C atoms, respectively. Blue color corresponds to the atoms in cubic diamond lattice. The atoms in the stacking faults (hexagonal diamond lattice) are shown in orange color. White color corresponds to the atoms within the dislocation cores that do not match any of the two mentioned perfect crystal lattice configurations.

3.3. Dissociation of 60^O perfect glide dislocations

In this section, we consider the predictions of all three MD potentials described above regarding the dissociation of the 60^O perfect glide dislocations. The processes addressed to here can

be referred to as local processes being primarily determined by local atomic configurations and rearrangements of bonds.

60^O dislocation dipoles have been inserted according to the procedure described above using the atom displacements calculated by formulas (1), in the glide set of the 3C-SiC lattice, i. e. between narrowly spaced [111] planes. Respective fragments of the simulation cell with inserted 60^O perfect glide dislocations with opposite Burgers vectors prior to any MD operation are shown in Fig. 3 a. We refer to these dislocations as terminated by carbon (left) and silicon (right), respectively, by the type of the atom that crowns the insertion plane.

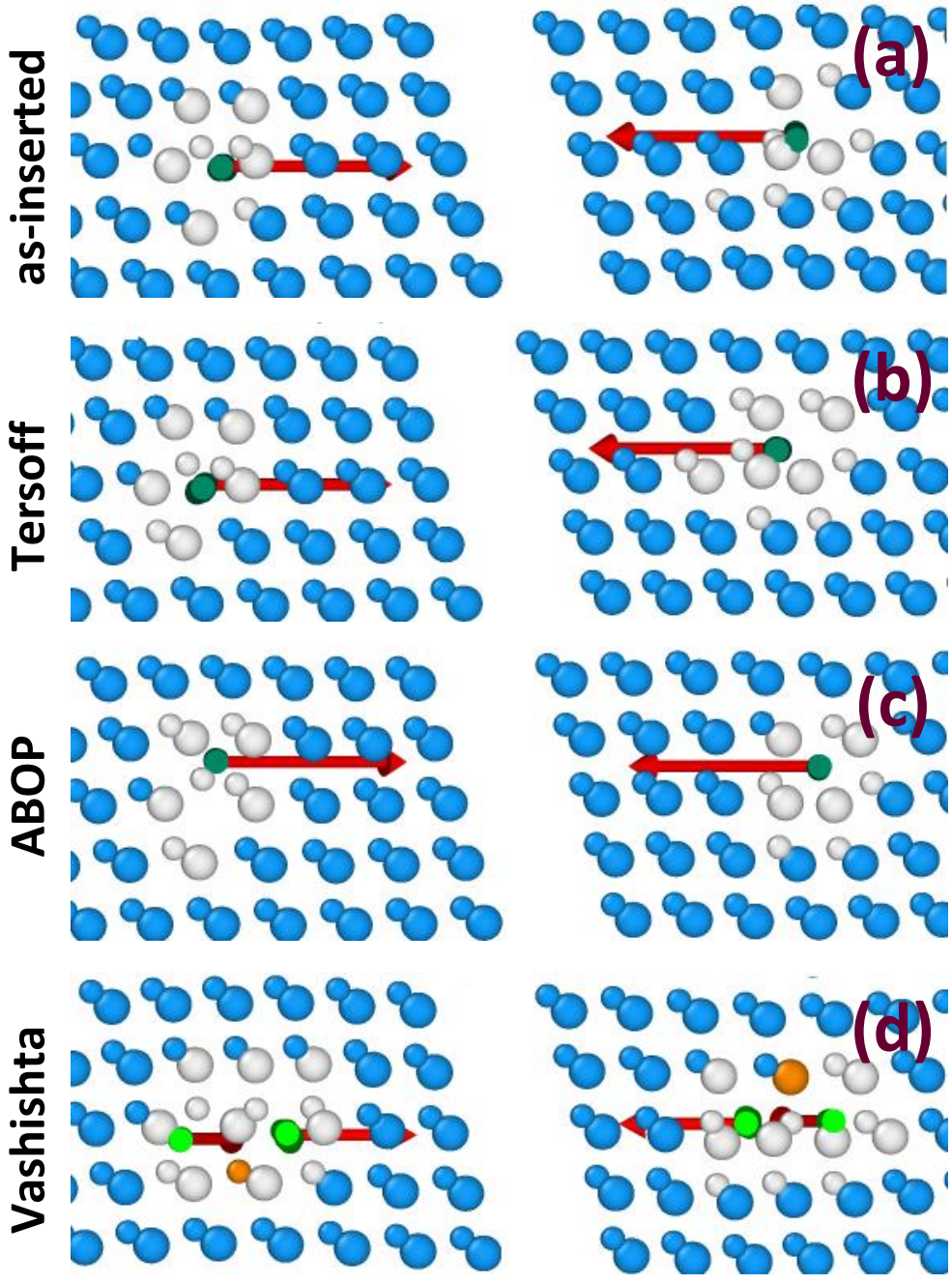

Fig. 3 Snapshots of the left and right parts of the 3C-SiC simulation cell after insertion of a pair of 60^O perfect dislocations (a) and after energy minimization procedure with Tersoff potential (b), ABOP (c) and Vashishta potential (d), respectively. Larger spheres represent Si atoms, while smaller ones correspond to C atoms, respectively. Flat dots indicate the projections of the dislocation lines of 60^O perfect or 30^O and 90^O partial dislocations. Arrows show the dislocation Burgers vectors. Blue color corresponds to the atoms in cubic diamond lattice. The atoms in the stacking faults (hexagonal diamond lattice) are shown in orange color. White color corresponds to the atoms within the dislocation cores that do not match any of the two mentioned perfect crystal lattice configurations.

Fig. 3 b-c shows OVITO images of the structure of simulation cell with 60^O dislocations after energy minimization procedure performed with each of the discussed MD potentials. As predicted by dislocation theory [33], energy minimization should result in the dissociation of each 60^O perfect dislocation into a pair of 30^O and 90^O Shockley partial dislocations. For cubic silicon carbide, the dissociation of 60^O perfect dislocations into 30^O–90^O partial pairs was reported experimentally [10, 11]. In case of atomistic simulations performed in this work, such dissociation is observed only for Vashishta potential (see Fig. 3 d), however, while both Tersoff potential and ABOP maintain the initial perfect structure of both C- and Si-terminated 60^O dislocations (see Fig. 3 b and c, respectively). This behavior can be related to the energetic barrier, which cannot be overcome by these both potentials.

To verify, whether the dissociation of 60^O perfect glide dislocations into pairs of 30^O and 90^O partials is energetically favorable with MD potentials, the energy vs the distance between 30^O and 90^O dislocations, which model the dissociated state of the 60^O perfect dislocations, has been calculated and compared to the energy of 60^O dislocations. Respective procedure has been implemented as follows. Pairs of 30^O and 90^O partials with various separations between them have been inserted in places of 60^O perfect dislocations, after which the simulation cell energy has been allowed to minimize by the LAMMPS code. The energies of the regions containing each partial dislocation pair have been calculated followed by subtraction of the energies of the same regions prior to the dislocations insertion. In this way, the energy values ΔE characterizing cores of 30^O and

90^O partial dislocations and interaction between them as well as the stacking fault energy (in case of Vashishta potential), have been extracted.

Fig. 4 shows the dependences of ΔE on the distance between the partial dislocations in the 30^O–90^O dislocation pair for all three potentials used. The initial points in these dependences for Tersoff potential and ABOP correspond to the perfect configuration of 60^O dislocation. The case of Vashishta potential is discussed separately below.

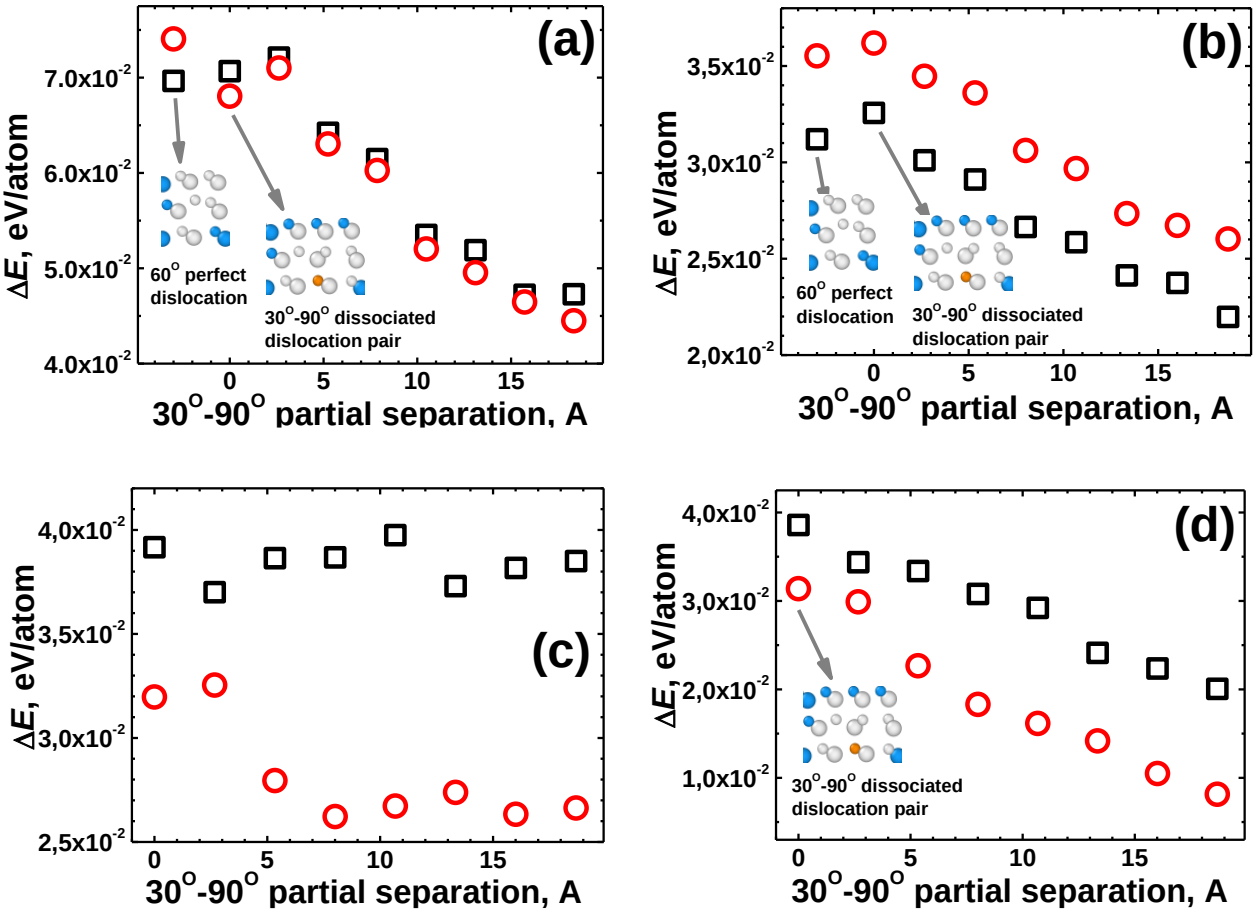

Fig. 4 Potential energy per atom vs separation of the pairs of 30^O and 90^O Shockley partial dislocations representing the dissociated states of perfect 60^O dislocations terminated by carbon (squares) and silicon (circles) atoms, calculated with Tersoff (a), ABOP (b) and Vashishta (c, d) potentials. In case of Vashishta potential, the result with (c) and without (d) account of the energy of stacking fault formed between the 30^O and 90^O dislocation pairs are presented. Insets in the graphs show the perfect 60^O or dissociated 30^O–90^O dislocation configurations

Results presented in Fig. 4 a and b demonstrate the existence of an energy barrier for the dissociation of perfect 60^O dislocations in 30^O–90^O dislocation pairs for both Tersoff potential and ABOP. Increase of the distance between the 30^O and 90^O partials beyond the energy barrier leads to the decrease of the value of ΔE, which testifies the tendency of their separation. Such tendency is correct from the physical point of view and corresponds to the existence of the repulsive force between the 30^O and 90^O dislocations in the dissociated pair [42]. Furthermore, we note that the Tersoff potential predicts equal energy values for both C- and Si-terminated 30^O–90^O partial pairs, while the energies calculated with ABOP are always smaller for carbon terminated dislocation pairs as compared to those of Si-terminated ones.

The situation in the case of Vashishta potential is more complicated than in the Tersoff potential and ABOP cases considered above. Perfect structures of 60^O dislocations cannot be stabilized with Vashishta potential. Dissociation of these dislocations in the pairs of 30^O and 90^O partials is always obtained by energy minimization (see Fig. 3 d). Increase of the distance between partials leads to small energy changes, especially in the case of carbon terminated dislocations, as shown by the graphs in Fig. 4 c. This means that Vashishta potential makes only a slight difference between various separation states of the 30^O and 90^O dislocations. Such situation is conditioned by the non-zero energy of the stacking fault, naturally forming between the 30^O and 90^O partials in the pair as a result of their insertion. Positive energy of stacking fault causes the tendency of a decrease of its extension thus creating effective attractive force between partial dislocations, which counterbalances the repulsive interaction force. Subtracting the stacking fault energy from the energy values corresponding to the data presented in Fig. 4 c, a similar trend to that obtained with other potentials is observed (see Fig. 4 d). Namely, the energy of 30^O and 90^O partial dislocations is predicted to decrease with the increase of their separation as conditioned by the existence of the repulsive interaction between them. At this, however, unlike the ABOP case, the energy of the system of carbon terminated dislocations is predicted to be higher than that for Si-terminated one.

3.4. MD simulation of the evolution of perfect and partial dislocation dipoles

In this section, the processes, which are determined by long-range interaction of dislocations are considered. In particular, we test three considered MD potentials with respect to their predictions on the evolution of dislocation dipoles composed of perfect 60^O – 60^O or partial 30^O – 30^O or 90^O – 90^O dislocation pairs with opposite Burgers vectors subjected to annealing at high temperature. In such systems, the stress fields created by dislocations induce long-range attractive interaction of them so that their motion toward each other with subsequent annihilation is expected as a result of MD simulated annealing.

The dislocation evolution during simulation runs is determined by the MD potential used. In particular, application of Tersoff potential to the simulation of 60^O dislocation dipoles does not result in any evolution for simulation times up to 6 ns and temperatures up to 2000 K (only local perturbations of the dislocation structures are observed increasing as the simulation temperature increases). Such behavior is pertinent to both perfect configuration of initial 60^O dislocation and dissociated one when 30^O and 90^O partials are in contact each with other having no separation between them (analogous to the structure shown in Fig. 3 d).

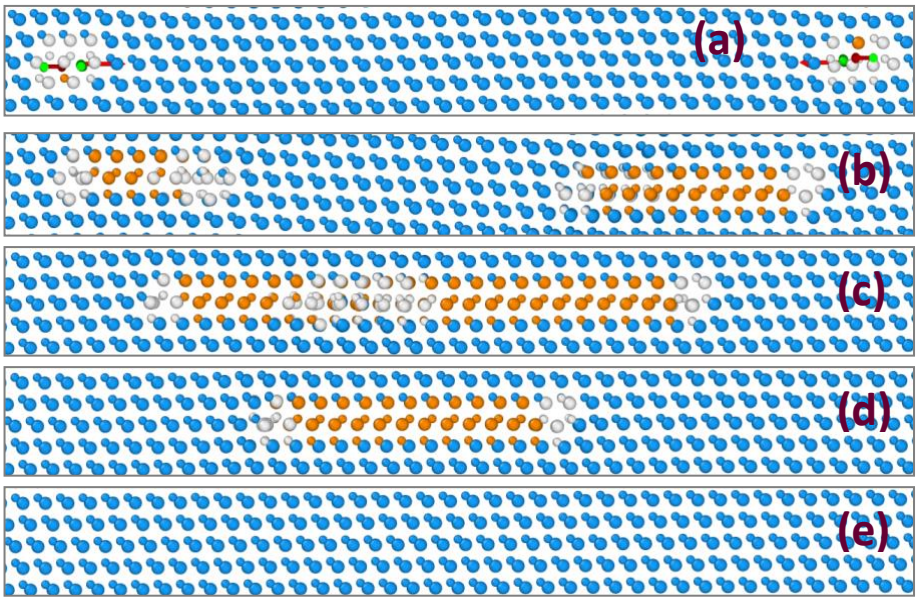

Fig. 5 Evolution of 60^O perfect dislocations in 3C-SiC at 2000 K simulated with Vashishta potential after energy minimization (a) and after 6 (b), 11.4 (c), 18 (d), and 24 (e) picoseconds of simulated time. Blue color

corresponds to the atoms in cubic diamond lattice. The atoms in the stacking faults (hexagonal diamond lattice) are shown in orange color. White color corresponds to the atoms within the dislocation cores that do not match any of the two mentioned perfect crystal lattice configurations.

In its turn, application of either of ABOP or Vashishta potential for MD simulations of the behavior of 60^O perfect dislocations demonstrates much better predictability and reliability of obtained results. Fig. 5 shows a series of OVITO images corresponding to different stages of the evolution of 60^O perfect dislocations in 3C-SiC obtained by simulations with Vashishta potential at 2000 K. Initial state is represented by a dislocation dipole comprising two 60^O glide dislocations with opposite Burgers vectors dissociated in pairs of 30^O and 90^O partials pairs by LAMMPS energy minimization procedure (see Fig. 5 a). Annealing at 2000 K results in the motion of partial dislocations caused by attraction of the dislocations with opposite Burgers vectors. Due to the difference in the relative motion velocities of 90^O and 30^O partials, they separate each from other leading to the formation of the clearly resolved stacking faults in each 30^O-90^O dislocation pair (Fig. 5 b). Prolonged annealing causes annihilation of the 90^O dislocations with opposite Burgers vectors with a formation of a single stacking fault between two 30^O partials first and approaching of the latter, annihilation and restoration of perfect lattice structure thereafter as demonstrated by the consecutive simulation snapshots presented in Fig. 5 c to e. The evolution scenario of 60^O dislocation dipole predicted with Vashishta potential fully coincides with expected one, which points out the applicability of this potential for the MD simulation study of the dislocations in 3C-SiC phase.

With application of ABOP, the evolution patterns equivalent to those depicted in Fig. 5 are seen but at a time scale several orders of magnitude larger than the one of Vashishta potential. First, the system needs time in order to overcome the energy barrier for dissociation of the initial perfect 60^O dislocation structures created by energy minimization procedure (see Fig. 4 b), while there is no such barrier in case of Vashishta potential. Second, the dislocation motion is much slower with

ABOP as will be discussed in more details below.

Relative motion velocities of dislocations have been studied performing MD simulations for the 30^O and 90^O dipoles separately. In particular, the simulations cell initially contained C- and Si-terminated 30^O or 90^O partial dislocations with opposite Burgers vectors in place of respective 60^O perfect dislocations. In these cases, stacking faults were naturally formed between the partials as a result of their insertion. The example of the simulation cell with inserted 30^O partial dislocation dipole is presented in Fig. 6. The evolution of this system at 2000 K simulated with molecular dynamics is presented by the OVITO images in Fig. 6 b to e. Long-range attraction of the partial dislocations induces their motion toward each other with subsequent annihilation in the meeting point and restoration of perfect cubic lattice structure. It should be emphasized that unlike the perfect 60^O dislocations, such behavior of partial dislocation dipoles is observed for all three potentials used but at different time scales indicating different velocities of the dislocation motion predicted by each potential. As the motion of partial dislocations is not uniform, we have characterized their velocities in terms of the migration distances and respective times, which can be summarized as presented in Table 2. At this, the migration distances of dislocations have been calculated over the lattice parameter *a*, provided by respective MD potential, with the step *l* equal to the shortest distance between the same-type atoms in the <112> direction, $d = a\frac{\sqrt{6}}{4}$, as can be obtained from simple geometrical analysis.

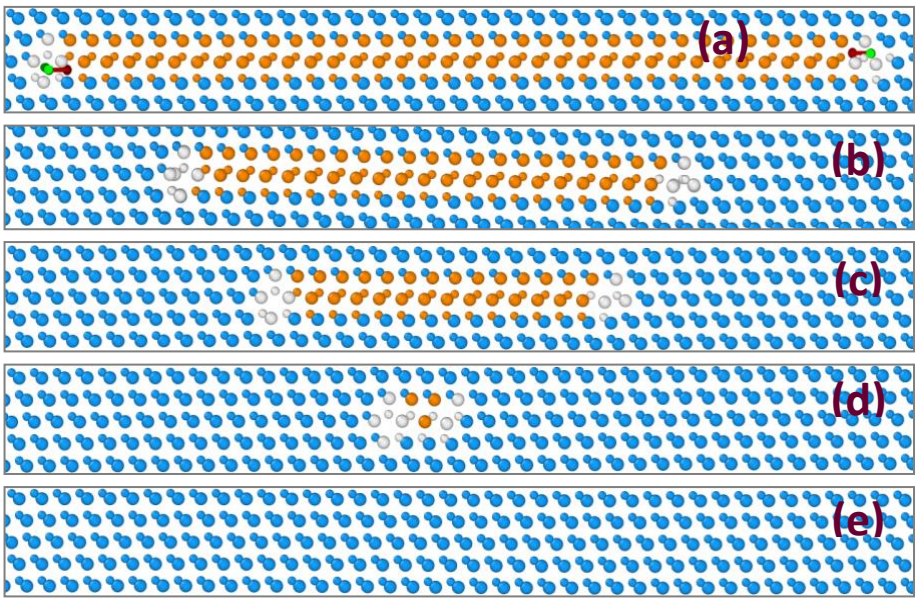

Fig. 6 Evolution of 30^O partial dislocations in 3C-SiC at 2000 K simulated with Vashishta potential after 0 (a), 6 (b), 12 (c), 18 (d), and 19.5 (e) picoseconds of simulated time. Blue color corresponds to the atoms in cubic diamond lattice. The atoms in the stacking faults (hexagonal diamond lattice) are shown in orange color. White color corresponds to the atoms within the dislocation cores that do not match any of the two mentioned perfect crystal lattice configurations.

The data in Table 2 enable to make the following conclusions. Motion velocity of the 90^O partial dislocation is predicted to be always higher than that of 30^O partial with the same atom type termination (carbon or silicon). At this, the velocities of 90^O dislocations predicted with Vashishta potential are about an order of magnitude higher than those obtained with other two potentials. The only exception is the 90^O Si-terminated partial dislocation simulated with Tersoff potential, for which no evolution could be detected up to the moment of its annihilation with arriving counterpart.

Table 2. Times and migration distances of partial dislocations characterizing their motion velocities calculated with three MD potentials at 2000 K

Simulated time	Potential	Dislocation type	Distance*
7.5 ps	Vashishta	90^O C-terminated	18.6819 Å
		90^O Si-terminated	37.3638 Å

		30^O C-terminated	16.013 Å
		30^O Si-terminated	18.6819 Å
75 ps	Tersoff	90^O C-terminated	26.2071 Å
		90^O Si-terminated	0 Å
	ABOP	90^O C-terminated	10.6781 Å
		90^O Si-terminated	13.3476 Å
750 ps	Tersoff	30^O C-terminated	10.4828 Å
		30^O Si-terminated	7.86213 Å
6 ns	ABOP	30^O C-terminated	2.66952 Å
		30^O Si-terminated	10.6781 Å

* The migration distances of dislocations are calculated over the lattice parameter *a* with the step *l* equal to the shortest distance between the same-type atoms in the <112> direction, $l = a\frac{\sqrt{6}}{4}$

The motion velocities of the 90^O and 30^O partial dislocations predicted with Vashishta potential are of the same order of magnitude for both C and Si atom termination. This means that their evolution is observed at the same time scale that is supported by the results discussed above with reference to Fig. 5. On the other hand, the motion velocities of 90^O partials are about an order and two orders of magnitude higher as compared to those of 30^O partials for the Tersoff potential and ABOP, respectively. Therefore, a clear separation in time between much faster evolution of the 90^O dislocation subsystem and much slower one of the 30^O dislocation subsystem are observed performing MD simulations with these potentials.

Finally, both Vashishta potential and ABOP predict higher motion velocities for the Si-terminated both 30^O and 90^O partial dislocations, while the Tersoff potential reveals quite the contrary behavior. The motion velocities of C- and Si-terminated dislocations of the same type (90^O or 30^O) are predicted to have comparable velocities, excluding the case of the 90^O Si-terminated

partial dislocation simulated with Tersoff potential considered above, for which no actual motion velocity could be predicted in our simulation system.

4. Discussion

Mutual comparison of results obtained by MD simulations with Tersoff, analytic bond order, and Vashishta potentials discussed above as well as comparison with DFT results enable to make conclusions about the degrees of the applicability of these potentials for the study of extended defects in 3C-SiC material.

According to the results of calculations summarized in Table 1, all three potentials predict sufficiently well the values of the lattice constant and cohesive energy of cubic Si carbide phase, although the values obtained with Tersoff potential look slightly poorer as compared to those provided with ABOP and Vashishta potential. We make also a reference to the paper by Chavoshi et al. [26], in which higher robustness of ABOP in predicting mechanical characteristics and elastic constants of 3C-SiC, especially the Voigt averages associated with dislocations, as compared to that of Tersoff potential, has been demonstrated. Besides, in this publication better agreement of the energy barrier for stacking fault formation given by ABOP, with DFT and *ab initio* calculations has been established. Moreover, we have found out in Section 3.4 that molecular dynamics simulations with Tersoff potential could not adequately predict the evolution of 60^{O} perfect dislocations in 3C-SiC material. As a result, we conclude that Tersoff potential is not sufficiently appropriate in application to the MD simulation study of extended defects in various configurations in 3C-SiC material.

Before making assessment of the applicability of other two potentials to model the extended defects in cubic silicon carbide, we would like to comment some more once on the hierarchy of the processes, which can be tackled by atomistic simulations with MD potentials. We can conventionally divide these processes to be “local”, for which the formation of local atomic configurations and dislocation cores determined by the evolution of bond structure is a primary

concern, and “non-local”, the rest of the processes, considered from the point of view of dislocation motion due to long-range interactions and extended stress fields. Of course, the motion of dislocations definitely contains the local aspect of atomic bond rearrangements, however, exact local mechanisms have an influence on only the speed but not the character of observed evolutions. Both types of processes were described in Sections 3.2, 3.3 and 3.4, the maintaining of core reconstruction and dissociation of the perfect structure of 60^{O} dislocations being the local processes and the dislocation motion the non-local one, respectively. Hereby, we analyze the correctness and reliability of the treatment of these processes provided by ABOP and Vashishta potential.

Formation of the core structures of partial dislocations as well as 60^{O} perfect dislocations corresponding to the local energy minimums for MD potentials, which has been considered in Sections 3.2 and 3.3, represent local processes, as has been already mentioned above. As can be seen from Figs. 2 and 3, ABOP and Vashishta potential provide principally different results on the possibility to stabilize the structures of the dislocation cores. In particular, change of the DFT provided core reconstruction is always observed with Vashihsta potential for all studied dislocation types. Moreover, no stable 60^{O} dislocation state can be obtained with this potential but only partially dissociated into 30^{O} and 90^{O} partial pair. The inequivalence of the treatment of local processes by ABOP and Vashishta potential is determined by peculiarities of their mathematical structures, in particular, how these potentials account for the interaction of the same-type atoms and the possibility of a formation of bonds between them. While ABOP favors formation of such bonds, the interaction between the atoms of the same elements is repulsive with Vashishta potential. This repulsion leads to the transformations of structures of 30^{O} and 90^{O} dislocations cores and loss of the core reconstructions provided by DFT calculations, as discussed in Section 3.2 (see Fig. 2).

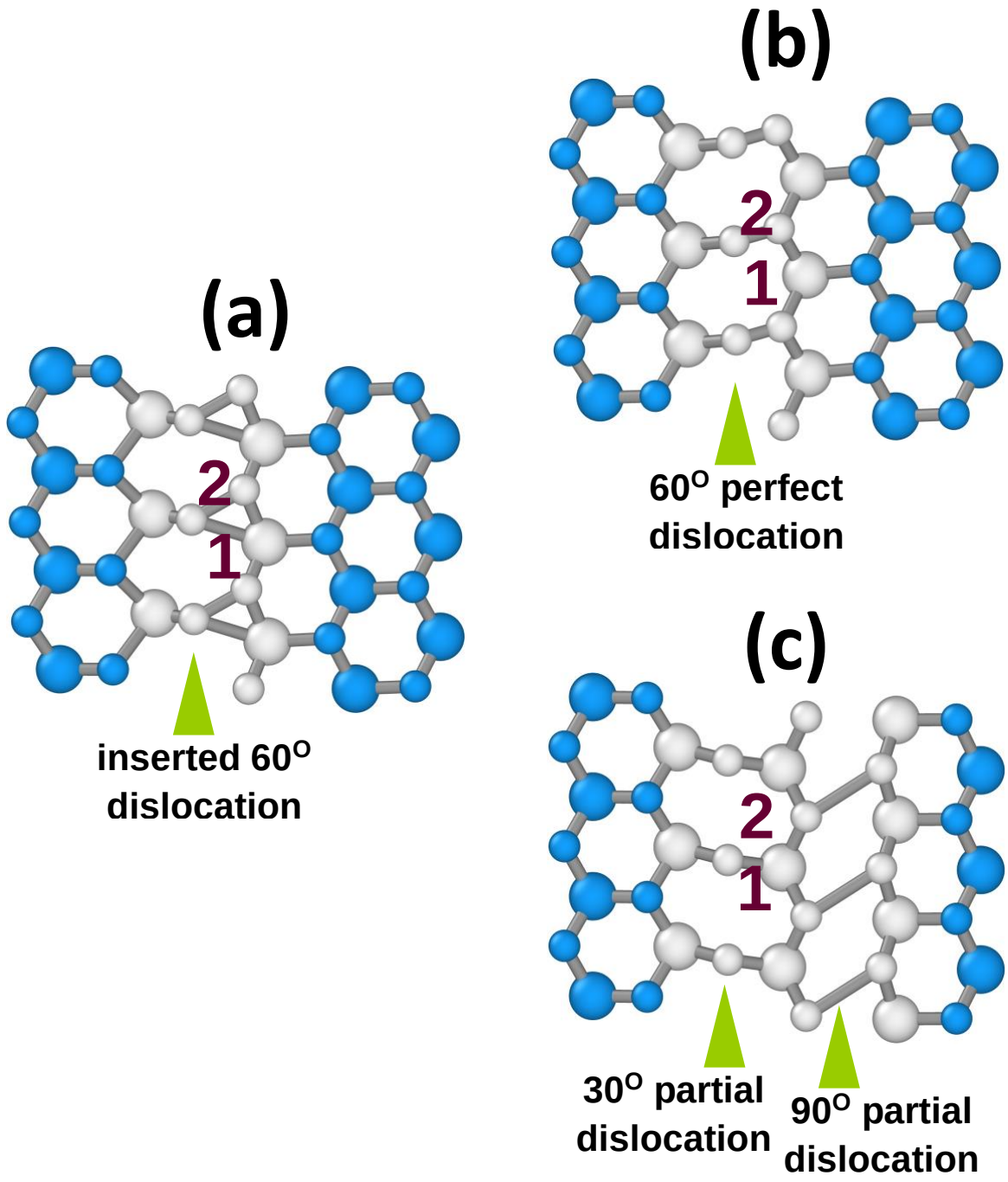

Fig. 7 Top view of the transformations of the initial structure of inserted in the simulation cell 60^{O} dislocation (a) resulted from MD energy minimization with ABOP (b) and Vashishta potential (c). Numbers point on the atom pairs that separate during transformations simulated with ABOP (1) and Vashishta potential (2), respectively. Arrows show the directions of respective dislocation lines

Fig. 7 illustrates the transformations of the initial core structure of a 60^{O} perfect dislocation (shown for the case of C-termination) inserted in the simulation cell, as a result of energy

minimization with ABOP and Vashishta potential. We notice here that the dislocation structures in Fig. 7 are viewed in the top-to-bottom direction, unlike the cases of Figs. 3, 5 and 6, where the simulation cell is presented in the frontal projection. In addition, atom connecting lines should not be necessarily considered as real bonds formed between these atoms but rather as representative indications of their relative proximity.

It is clearly seen from Fig. 7 a that the initial core of the 60^O dislocation contains triangles of closely spaced atoms, two of which are of the same type (carbon atoms for the C-terminated 60^O perfect dislocation). Since ABOP potential favors the C–C atom attraction, the transformation of initial state as a result of energy minimization takes place as demonstrated in Fig. 7 b, i. e. the distances 1 between the C and Si atoms in the central atomic triangles increase leading to the formation of a 60^O perfect dislocation core structure.

On the other hand, the structure of the 60^O perfect dislocation containing C–C bonds cannot be maintained by Vashishta potential in view of the repulsion created by this potential between the atoms of the same type. This issue is additionally illustrated by the value of the energy of a 60^O perfect dislocation core obtained by a stabilization with ABOP or Tersoff potential, calculated with Vashishta potential, which exceeds that of the 30^O and 90^O dissociated pair by about 0.03 eV/atom. Repulsion between the carbon atoms in the triangles of closely spaced atoms of the inserted 60^O dislocation depicted in Fig. 7 a causes the tendency of their separation (increase of the distance 2). In its turn, this leads to the dissociation of initial 60^O dislocation in the pair of 30^O and 90^O partials as shown in Fig. 7 c.

Generalizing, one may conclude that Vashishta potential cannot provide reliable description of the local processes, in which repulsive interactions between closely spaced atoms of the same types predicted by this potential play significant role and is not counterbalanced by the attraction between the atoms of different types. On the other hand, ABOP, which more correctly describes the same-type atom interaction and formation of bonds between them, better reproduce in particular, the stabilization of the perfect structure of 60^O dislocation discussed above, as well as the

configurations of the partial dislocation cores better corresponding to those obtained by DFT simulations [12]. Therefore, one is enabled to qualify the analytic bond order potential as being more suitable to use for simulations of the local processes in 3C-SiC material.

Despite differences in the descriptions of local processes given by ABOP and Vashishta potential, one may state based on the results presented in Section 3.4 that the predictions regarding non-local processes provided by both potentials are qualitatively equivalent. Both potentials predict higher motion velocities of 90^{O} partials as compared to 30^{O} dislocations in agreement with DFT calculations [12]. Although the relation of the velocities of Si- and C-terminated dislocations obtained from molecular dynamics is contrary to respective DFT result, according to which faster motion of C-terminated dislocations should be observed [12], however, there are experimental indications supporting our MD results and demonstrating that Si-terminated partial dislocations in silicon carbide move faster than C-terminated ones [42].

In view of the larger cut-off radius and, hence, higher number of atomic interactions to be treated, it takes remarkably longer in real time to perform a single time step of MD simulations with Vashishta potential as compared to that with ABOP. However, Vashishta potential provides much faster simulated kinetics of the non-local processes presumably resulted from the repulsion interaction in the Si – Si and C – C atom pairs. This accelerated kinetics with Vashishta leads to that at least an order of magnitude smaller number of time steps is required to see equivalent progress in the system evolution than in the analytic bond order potential case. The tests also demonstrate that reasonable acceleration of process kinetics with ABOP by raise of the simulation temperature (despite the mentioned above noticeable overestimation of the melting temperature with this potential) is not achievable due to the SiC amorphisation. In this respect, MD simulations of non-local processes with Vashishta potential are advantageous from the point of view of the computation time load and the speed of results accumulation.

Based on the discussion presented we should conclude that neither ABOP, nor Vashishta potential represents an ideal solution for molecular dynamics simulations related to the extended

defects in 3C-SiC material. Instead, their synergetic application is suggested, in which general picture of the system evolution comprising long-distance interaction and motion of dislocations and stacking faults is modeled with Vashishta potential with gain in computation time, while local processes, such as bond rearrangements, formation of local atomic configurations and dislocation core structures are studied performing ABOP based simulations. We should also notice that we expect the proposed approach to be highly efficient for modeling of not only simple systems composed of dislocations and stacking faults, but also of more complex defects in 3C-SiC such as twin regions, polytype inclusions and antiphase domains, for which the stacking faults and bounding partial dislocations can be regarded as elementary building blocks.

5. Conclusion

In conclusion, we have made a systematic study of the applicability of three MD potentials, namely Tersoff, analytic bond order and Vashishta potentials, to the simulation of the evolution of systems composed of 60^{O} perfect as well as 30^{O} and 90^{O} Shockley partial dislocations and stacking faults in 3C-SiC phase. Poorer, as compared to other potentials, reproduction of 3C-SiC characteristics and dislocation dynamics with Tersoff potential qualify it as less appropriate for the study of the evolution of dislocations and their complexes in cubic Si carbide. On the other hand, predictions of the large-scale behavior of dislocations and stacking faults given by ABOP and Vashishta potentials are qualitatively the same, the difference being in the time scale of process evolution. The time scale of simulations with Vashishta potential is about one to three orders of magnitude smaller as compared to that of ABOP, which is determined by its mathematical structure causing repulsion between the atoms of the same types. Such acceleration of process kinetics with Vashishta potential leads to significant gain in the real time of computation due to smaller number of time steps required. In its turn, ABOP is more correct in prediction of the structure of dislocation cores and evolution of local atomic configurations. In this respect, synergetic use of both Vashishta potential and ABOP is suggested for the detailed molecular dynamics simulation study of the

behavior and properties of extended defects in 3C-SiC material. Namely, Vashishta potential is better to apply to track the large-scale evolution of system characterized in terms of the long-distance dislocations and stacking faults transformations. In its turn, local processes, such as bond rearrangements, formation of local atomic configurations and dislocation core structures should be studied performing simulations with ABOP as provided more reliable predictions. In addition, analytic bond order potential can be used to confirm from time to time the consistency of ABOP and Vashishta results. It should be noticed as well that the efficiency of proposed simulation approach is expected also in study of more complex defects in 3C-SiC such as twin regions, polytype inclusions and antiphase domains, for which the stacking faults and bounding partial dislocations are as elementary building blocks.

Acknowledgement

Authors acknowledge EU for funding the CHALLENGE project (3C-SiC Hetero-epitaxiALLy grown on silicon compliancE substrates and 3C-SiC substrates for sustaiNable wide-band-Gap powEr devices) within the EU's H2020 framework program for research and innovation under grant agreement n. 720827.

Conflicts of interest

The authors declare that they have no conflict of interest.

References

[1] Piluso N, Severino A, Camarda M, Canino A, La Magna A and La Via F 2010 Optical investigation of bulk electron mobility in 3C–SiC films on Si substrates *Appl. Phys. Lett.* **97** 142103

[2] Tachibana T, Kong H S, Wang Y C and Davis R F 1990 Hall measurements as a function of temperature on monocrystalline SiC thin films *J. Appl. Phys.* **67** 6375-6381

[3] Hwang J D, Fang Y K, Song Y J and Yaung D N 1996 High mobility β-SiC epilayer prepared by low-pressure rapid thermal chemical vapor deposition on a (100) silicon substrate *Thin Solid Films* **272** 4-6

[4] Schoner A, Krieger M, Pensl G, Abe M and Nagasawa H 2006 Fabrication and characterization of 3C-SiC-based MOSFETs *Chem. Vap. Depos.* **12** 523-530

[5] Takahashi M, Im S-S, Madani M and Kobayashi H 2008 Nitric acid oxidation of 3C-SiC to fabricate MOS diodes with a low leakage current density *J. Electrochem. Soc.* **155** H47-H51

[6] Constant A, Camara N, Placidi M, Decams J-M, Camassel J and Godignon P 2011 Interfacial properties of oxides grown on 3C-SiC by rapid thermal processing *J. Electrochem. Soc.* **158** G13-G19

[7] La Via F, Severino A, Anzalone R, Bongiorno C, Litrico G, Mauceri M, Schoeler M, Schuh P and Wellmann P 2018 From thin film to bulk 3C-SiC growth: Understanding the mechanism of defects reduction *Mater. Sci. in Semicond. Proc.* **78** 57-68

[8] Polychroniadis E, Syvajarvi M, Yakimova R and Stoemenos J 2004 Microstructural characterization of very thick freestanding 3C-SiC wafers *J. Cryst. Growth* **263** 68-75

[9] Vasiliauskas R, Marinova M, Syväjärvi M, Polychroniadis E K and Yakimova R 2014 Polytype transformation and structural characteristics of 3C-SiC on 6H-SiC substrates *J. Cryst. Growth* **395** 109-115

[10] Kaiser U and Khodos I I 2002 On the determination of partial dislocation Burgers vectors in fcc lattices and its application to cubic SiC films *Phil. Mag.* **82** 541-551

[11] Wen C, Wang Y M, Wan W, Li F H, Liang J W and Zou J 2009 Nature of interfacial defects and their roles in strain relaxation at highly lattice mismatched 3C-SiC/Si (001) interface *J. Appl. Phys.* **106** 073522

[12] Blumenau A T 2002 The modelling of dislocations in semiconductor crystals *PhD Thesis* University of Padeborn

[13] Lebedev A A, Abramov P L, Lebedev S P, Oganesyan G A, Tregubova A S and Shamshur D

V 2009 Influence of the defect density (twins boundaries) on electrical parameters of 3C-SiC epitaxial films Physica B **404** 4758-4760

[14] Song X, Michaud J F, Cayrel F, Zielinski M, Portail M, Chassagne T, Collard E and Alquier D 2010 Evidence of electrical activity of extended defects in 3C–SiC grown on Si *Appl. Phys. Lett.* **96** 142104

[15] Deretzis I, Camarda M, La Via F and La Magna A 2012 Electron backscattering from stacking faults in SiC by means of ab initio quantum transport calculations *Phys. Rev.* B **85** 235310

[16] Nagasawa H, Yagi K, Kawahara T, Hatta N and Abe M 2006 Hetero- and homo-epitaxial growth of 3C-SiC for MOS-FETs *Microelectron. Eng.* **83** 185-188

[17] Nagasawa H, Kawahara T, Yagi K, Hatta N, Uchida H, Kobayashi M, Reshanov S, Esteve R and Schöner A 2012 High quality 3C-SiC substrate for MOSFET fabrication *Mater. Sci. Forum* **711** 91-98

[18] Tersoff J 1989 Modeling solid-state chemistry: Interatomic potentials for multicomponent systems *Phys. Rev.* B **39** 5566-5568

[19] Tersoff J 1990 Carbon defects and defect reactions in silicon *Phys. Rev. Lett.* **64** 1757-1760

[20] Tersoff J 1994 Chemical order in amorphous silicon carbide *Phys. Rev.* B **49** 16349-16352

[21] Erhart P and Albe K 2005 Analytical potential for atomistic simulations of silicon, carbon, and silicon carbide *Phys. Rev.* B **71** 035211

[22] Vashishta P, Kalia R K, Nakano A and Rino J P 2007 Interaction potential for silicon carbide: A molecular dynamics study of elastic constants and vibrational density of states for crystalline and amorphous silicon carbide *J. Appl. Phys.* **101** 103515

[23] Shimojo F, Ebbsjö I, Kalia R K, Nakano A, Rino J P and Vashishta P 2000 Molecular dynamics simulation of structural transformation in silicon carbide under pressure *Phys. Rev. Lett.* **84** 3338-3341

[24] Li W, Yao X and Zhang X 2018 Planar impacts on nanocrystalline SiC: a comparison of different potentials *J. Mater. Sci.* **53** 6637-6651

[25] Li W, Hahn E N, Yao X, Germann T C and Zhang X 2019 Shock induced damage and fracture in SiC at elevated temperature and high strain rate *Acta Mater.* **167** 51-70

[26] Chavoshi S Z and Luo X 2016 Molecular dynamics simulation study of deformation mechanisms in 3C–SiC during nanometric cutting at elevated temperatures *Mater. Sci. Eng.* A **654** 400-417

[27] Goel S, Stukowski A, Luo X, Agarwal A and Reuben R L 2013 Anisotropy of single-crystal 3C-SiC during nanometric cutting *Model. Simul. Mater. Sci. Eng.* **21** 065004

[28] Wojdyr M, Khalil S, Liu Y and Szlufarska I 2010 Energetics and structure of $\langle 0\,0\,1 \rangle$ tilt grain boundaries in SiC *Model. Simul. Mater. Sci. Eng.* **18** 075009

[29] Stillinger F H and Weber T A 1985 Computer simulation of local order in condensed phases of silicon *Phys. Rev.* B **31** 5262-5271

[30] Plimpton S 1995 Fast parallel algorithms for short-range molecular dynamics *J. Comput. Phys.* **117** 1-19

[31] Yan W J, Gao T H, Guo X T, Qin Y X and Xie Q 2013 Melting kinetics of bulk SiC using molecular dynamics simulation *Sci. China – Phys. Mech. Astron.* **56** 1699–1704

[32] Stukowski A 2010 Visualization and analysis of atomistic simulation data with OVITO–the Open Visualization Tool *Model. Simul. Mater. Sci. Eng.* **18** 015012

[33] Hirth J P and Lothe J 1982 *Theory of Dislocations* (Malabar: Krieger Publishing Company)

[34] Tong L, Mehregany M and Matus L G 1992 Mechanical properties of 3C silicon carbide *Appl. Phys. Lett.* **60** 2992-2994

[35] Haynes W M 2014 *CRC Handbook of Chemistry and Physics: a Ready-Reference Book of Chemical and Physical Data* (Boca Raton: CRC Press)

[36] Harrison W A 1980 *Electronic Structure and the Properties of Solids: The Physics of the Chemical Bond* (San Francisco: Freeman)

[37] Adamski R F and Merz K M 1959 Synthesis and crystallography of the wurtzite form of silicon carbide *Z. Kristallogr.* **111** 350-361

[38] Scalise E, Marzegalli A, Montalenti F and Miglio L 2019 Temperature-dependent stability of polytypes and stacking faults in SiC: reconciling theory and experiments *Phys. Rev. Applied* **12** 021002

[39] Hong M H, Samant A V and Pirouz P 2000 Stacking fault energy of 6H-SiC and 4H-SiC single crystals *Philos. Mag.* A **80** 919-935

[40] Ning X G and Ye H Q 1990 Experimental determination of the intrinsic stacking-fault energy of SiC crystals *J. Phys.: Condens. Matter* **2** 10223-10225

[41] Blumenau A T, Fall C J, Jones R, Öberg S, Frauenheim T and Briddon P R 2003 Structure and motion of basal dislocations in silicon carbide *Phys. Rev.* B **68** 174108

[42] Skowronski M and Ha S 2006 Degradation of hexagonal silicon-carbide-based bipolar devices *J. Appl. Phys.* **99** 011101